Meat and Muscle Biology™

Prenatal Heat Stress Programs Skeletal Muscle Metabolism and Myogenesis in Dairy Heifers

Donghun Kang[1], Erika P. Eckhardt[1], Sena Field[2], Jimena Laporta[2]*, and Jongkyoo Kim[1,3]*

[1]Department of Animal Science, Michigan State University, East Lansing, MI 48823, USA
[2]Department of Animal and Dairy Sciences, University of Wisconsin–Madison, Madison, WI 53706, USA
[3]Department of Food Science and Human Nutrition, Michigan State University, East Lansing, MI 48823, USA
*Corresponding authors. Email: jlaporta@wisc.edu (Jimena Laporta) and kimjon48@msu.edu (Jongkyoo Kim)

Abstract: Heat stress (HS) during late gestation alters fetal development, potentially having lasting effects on skeletal muscle growth and metabolism in cattle. This study investigated molecular and cellular adaptations of the semitendinosus muscle in dairy heifer calves exposed to in utero HS (IUHS) or in utero cooling (IUCL) during the final 54 d of gestation. Muscle samples were collected at birth (day 0 [d 0]; before colostrum feeding) and postweaning (day 63 [d 63]; $n = 8$/group/time). Gene expression and protein abundance of heat-shock proteins (HSP), mitochondrial markers, and myogenic regulatory factors were analyzed by real-time quantitative polymerase chain reaction and Western blotting, while immunohistochemistry was used to assess paired box protein 7$^+$ (PAX7$^+$) satellite-cell abundance and myosin heavy chain fiber-type composition.

At d 0, IUHS muscle exhibited higher HSP60 abundance and greater peroxisome proliferator-activated receptor alpha and perilipin 5 messenger RNA (mRNA) expression, associated with altered mitochondrial quality-control and fatty-acid oxidative signaling. Adenosine monophosphate-activated protein kinase abundance exhibited a temperature × time interaction that was greater in IUHS than IUCL at d 0 but not different at d 63. Peroxisome proliferator-activated receptor gamma coactivator 1-alpha abundance was greater in IUHS calves ($P < .001$), whereas HSP60 protein abundance did not differ between treatments at d 63. At d 63, mitochondrial DNA content was reduced in IUHS muscle ($P = .005$). HSP27 protein abundance exhibited a temperature × time interaction ($P = .001$) that was lower in IUHS than IUCL at d 63 ($P = .003$) but not different at d 0. HSP70 protein abundance exhibited a temperature × time interaction ($P < .001$), with no difference between IUHS and IUCL at birth (d 0) but lower abundance in IUHS than IUCL at d 63. IUHS dairy heifers exhibited elevated PAX7$^+$ satellite cells ($P = .005$), greater *myoblast determination protein 1* and *myogenin* mRNA, and had a higher proportion of type I ($P = .020$) and type IIX ($P = .027$) fibers, with fewer type IIA fibers ($P < .001$). These findings indicate that prenatal heat exposure remodels skeletal muscle fiber-type composition and myogenic programming. Although IUHS heifers exhibited a greater proportion of type I fibers, they also showed an increased proportion of type IIX fibers with fewer type IIA fibers, consistent with redistribution among fast-fiber subtypes rather than a uniform shift toward oxidative fiber development. The increase in PAX7$^+$ satellite cells further supports altered myogenic regulation in IUHS offspring.

Keywords: in utero heat stress, skeletal muscle development, satellite cells, mitochondrial remodeling, muscle fiber types
Meat and Muscle Biology 10(1): 20990, 1–18 (2026) **doi:10.22175/mmb.20990**
Submitted 15 October 2025 Accepted 2 February 2026

Introduction

Heat stress (HS) has become a significant challenge in the livestock industry, exacerbated by ongoing climate change (Thornton et al., 2021). Severe environmental stressors affect animal physiology, immune function, and metabolism at all stages of life, ultimately compromising growth, health, and productivity. Despite its importance, research on prenatal HS in bovine species remains limited, primarily due to the challenges and complexity associated with controlled experimental models. This difficulty includes the

© 2026 Kang, et al.
This is an open access article distributed under the CC BY license (https://creativecommons.org/licenses/by/4.0/)

isolation of direct fetal effects from maternal influences and the long production cycle of cattle, requiring more than 2 y to assess offspring production outcomes. However, dairy and beef cattle are increasingly exposed to periods of extreme heat, and climate change is expected to increase the frequency of hot days and heat waves, thereby elevating the risk of HS and underscoring the urgent need to understand the physiological and molecular consequences of HS to develop effective mitigation strategies for livestock production (Das et al., 2016; Summer et al., 2019; Cartwright et al., 2023).

Exposure to prenatal HS in late gestation reduces birth and weaning weights in dairy calves, with smaller and shorter heifers until 1 y of age (Monteiro et al., 2016; Dado-Senn et al., 2022). Similarly, a reduction in organ weight has been exhibited for the liver, heart, and gastrointestinal tract in addition to enlarged adrenal glands and immune-related organs, suggesting alterations in developmental programming that may influence metabolic, immune function, and overall growth efficiency (Ahmed et al., 2021; Dado-Senn et al., 2022). HS is believed to influence muscle growth potential in mammals and poultry, yet findings across studies remain inconsistent. Reports in rodents (Frier and Locke, 2007), porcine (Montilla et al., 2014; Gao et al., 2015; Ganesan et al., 2017), and poultry (Ma et al., 2018) indicate that HS negatively affects muscle development, physiology, and immune responses. However, other studies suggest that HS may enhance muscle growth potential through mechanisms such as increased expression and abundance of myosin heavy chain (MyHC) isoforms and the mechanistic target of rapamycin (mTOR) pathway (Uehara et al., 2004; Xu et al., 2022; Kim and Kim, 2023) in rodents, poultry, and bovine myocytes relatively, as well as modifications in the satellite-cell population in bovine (Kim et al., 2023) and avian (Halevy et al., 2001; Xu et al., 2022) species. Additionally, transcriptional changes in skeletal muscle have been reported in heat-stressed cattle during the finishing stage, indicating potential anabolic adaptations (Reith et al., 2022). However, the mechanisms underlying these responses remain largely unknown, necessitating targeted studies to bridge the existing knowledge gaps. In particular, the impact of prenatal HS on skeletal muscle development in offspring remains poorly understood in cattle. Johnson et al. (2020) reviewed the consequences of in utero HS (IUHS) in swine, summarizing evidence that prenatal HS can be associated with reduced birth weight, slower postnatal growth, and altered body composition. Consistent with this, gestational HS has been shown to decrease lean mass while increasing adipose tissue deposition in pigs (Boddicker et al., 2014) and to increase the adipose-to-muscle ratio in sows and their offspring (Lucy and Safranski, 2017). However, given the species-specific differences in thermoregulation and metabolic adaptation, findings from other species cannot be directly extrapolated to cattle.

In the United States, the dairy-influenced beef sector is expanding, and this trend is expected to continue (Pereira et al., 2024; Brito et al., 2025). Understanding late-gestation HS impacts on skeletal muscle development in offspring of Holstein dairy cows is essential for optimizing growth performance in cattle destined for the feedlot amid the warming climate.

This study aims to examine the impact of IUHS during the late-gestation period on skeletal muscle development, with a focus on stress responses and skeletal muscle growth potential. We hypothesized that IUHS induces comprehensive developmental programming in fetal skeletal muscle as an adaptation to prenatal stress. Specifically, we predicted that this environment simultaneously alters stress response pathways, muscle-fiber-type distribution, and metabolic regulator expression, leading to a modified growth trajectory that persists through the early postweaning period.

Materials and Methods

Animal management and treatments

The skeletal muscle samples used in this study were obtained from a previously published experiment by Dado-Senn et al. (2021), which investigated the effects of late-gestation IUHS on dairy heifer growth and organ development. Briefly, pregnant multiparous Holstein cows ($n = 82$) were assigned to either HS (HT, $n = 41$) or cooled (CL, $n = 41$) treatment during the last 54 d ± 5 d of gestation. Dairy heifer calves born to these dams were considered IUHS ($n = 36$) or in utero cooled (IUCL, $n = 37$) and were managed identically as a cohort postnatally. A subset of these dairy heifers was euthanized at birth (day 0 [d 0], $n = 8$/in utero treatment group) or 1-wk postweaning from milk replacer (weaned at day 56 [d 56] and sampling occurred 7 d later at day 63 [d 63], $n = 8$/in utero treatment group, born between September 26 and October 2) for organ and tissue collection. For the present study, skeletal muscle samples collected from these dairy heifers were used for further analysis.

All animal procedures were conducted in accordance with the Institutional Animal Care and Use Committee protocol (#201910599). Further details on animal management and animal euthanasia processes are available in Dado-Senn et al. (2021).

Skeletal muscle sample collection

Time from euthanasia to completion of muscle tissue collection was approximately 30 min. For birth euthanasia, the semitendinosus (ST) muscle was collected before colostrum feeding to ensure the tissue was in a fasted state. For weaning euthanasia, dairy heifers were fasted overnight before sample collection to standardize metabolic conditions across groups. Further details on tissue collection procedures and handling are available in Dado-Senn et al. (2021).

Following euthanasia at d 0 and d 63, the ST muscle was carefully dissected from both hind limbs under standardized procedures to ensure consistency in sample collection. The ST muscle was sampled at the midbelly, with tissue collected from the central internal deep region, representing a mixed fiber-type area between the superficial, predominantly glycolytic (white) portion and the deeper, more oxidative (red) portion. Sampling was performed using consistent anatomical landmarks across all animals to minimize within-muscle variability while avoiding visible connective tissue and fat. Samples were collected at a uniform depth and orientation. The muscle was excised immediately postmortem, weighed, and processed for downstream analyses. A 0.5×0.5-cm^3 tissue portion was fixed in 10% neutral buffered formalin (NBF; Sigma-Aldrich, St. Louis, MO, USA) overnight, transferred to $1 \times$ phosphate-buffered saline (PBS, Waltham, MA, USA), and stored at 4°C until paraffin embedding presentation. A second tissue portion was preserved immediately after collection in the embedding medium for cryostat sectioning (Tissue-Tek® OCT Compound; Sakura Finetek, Torrance, CA, USA) and placed in dry ice. Approximately 200 mg of tissue was cut and rinsed in cold sterile PBS, dried, and stored in RNA later (Invitrogen; AM7020, Grand Island, NY, USA) for 24 h at room temperature and then at −80°C until RNA extraction. Another approximate 200 mg was snap-frozen in liquid nitrogen for RNA and protein isolation. The frozen samples were shipped overnight on dry ice to Michigan State University (East Lansing, MI, USA) for protein, gene expression, and histological analyses.

Messenger RNA extraction and real-time quantitative polymerase chain reaction

Total RNA was extracted from the ST muscle using TRIzol® reagent (Invitrogen, Carlsbad, CA, USA), following previously described methods (Kim et al., 2018). The messenger RNA (mRNA) concentration and purity were measured using a NanoDrop™ One/OneC Microvolume UV-Vis Spectrophotometer (Thermo Fisher Scientific) at absorbances of 260 nm and 280 nm. Samples with a 260 to 280 ratio between 1.90 and 2.05 were considered acceptable. Complementary DNA (cDNA) was synthesized using the High-Capacity cDNA Reverse Transcription Kit (Applied Biosystems, Foster City, CA, USA) with the ProFlex™ PCR System (Applied Biosystems), following the manufacturer's instructions. Relative gene expression levels were determined by real-time quantitative polymerase chain reaction (PCR) using the QuantStudio 6 Pro System (Thermo Fisher Scientific). The relative expression levels of heat-shock proteins (HSP), activating transcription factor 4 (*ATF4*), myogenic regulatory factors (*MRF*), *MYH7*, and adipogenic/lipogenic factors were measured relative to the quantity of ribosomal protein subunit 9 (*RPS9*) and hydroxymethylbilane synthase (*HMBS*) mRNA in total RNA. Target gene expression was normalized using the geometric mean of 2 housekeeping genes, *RPS9* and *HMBS*. *RPS9* served as the primary endogenous control, and its stable expression was validated by comparison with *HMBS*. Relative quantification of the target cDNA was assessed using TaqMan Fast Advanced Master Mix (Applied Biosystems, Foster City, CA, USA) and TaqMan Gene Expression Assays (Thermo Fisher Scientific; Tables 1 and 2). Duplicate assays were performed following the manufacturer's recommended thermal cycling parameters, consisting of 45 cycles of 15 s at 95°C and 1 min at 60°C. All PCR and cycle-threshold (Ct) value analyses were conducted using the QuantStudio 6 Pro System. Relative mRNA expression of each target gene was calculated using the comparative Ct method. Expression values were normalized to the geometric mean of the reference genes *RPS9* and *HMBS*, and the mean value of the IUCL group at d 0 was used as the calibrator.

Mitochondrial DNA quantification

Total DNA was extracted from the ST muscle using the Wizard® Genomic DNA Purification Kit (Promega, Madison, WI, USA). The relative mitochondrial DNA (mtDNA) content, expressed as the ratio of mitochondrial to nuclear DNA, was determined by

Table 1. List of TaqMan® assay for reverse transcription quantitative real-time polymerase chain reaction assays in skeletal muscle samples.

Gene Symbol	TaqMan® Assay ID	Manufacturer[1]	Target Description
RPS9	Bt03272016_m1	Thermo Fisher	Ribosomal protein*
ATF4	Bt03221057_m1	Thermo Fisher	Activating transcription factor 4
HSP27	Bt03220563_m1	Thermo Fisher	Heat-shock protein 27
HSP60	Bt04301470_g1	Thermo Fisher	Heat-shock protein 60
HSP70	Bt03292670_m1	Thermo Fisher	Heat-shock protein 70
HMBS	Bt03234763_m1	Thermo Fisher	Hydroxymethylbilane synthase*
IGF-1	Bt03252282_m1	Thermo Fisher	Insulin-like growth factor 1
Myf5	Bt03223134_m1	Thermo Fisher	Myogenic factor 5
MyoD	Bt03244740_m1	Thermo Fisher	Myoblast determination protein 1
MyoG	Bt03258928_m1	Thermo Fisher	Myogenin
MYH7	Bt03224257_m1	Thermo Fisher	Myosin heavy chain type I
C/EBPα	Bt03224529_s1	Thermo Fisher	CCAAT/enhancer-binding protein alpha
PPARα	Bt03220821_m1	Thermo Fisher	Peroxisome proliferator-activated receptor alpha
PPARγ	Bt03217547_m1	Thermo Fisher	Peroxisome proliferator-activated receptor gamma
PGC-1α	Bt01208835_m1	Thermo Fisher	Peroxisome proliferator-activated receptor gamma coactivator 1-alpha
PLIN5	Bt03271846_m1	Thermo Fisher	Perilipin 5

[1]This table summarizes the TaqMan® assays used for quantifying gene expression. All assays were purchased from Thermo Fisher Scientific and designed for use with Bos taurus gene targets.

*Reference genes.

Table 2. TaqMan® probes and primers used for reverse transcription quantitative real-time polymerase chain reaction assays.

Gene	Primer and Probe Sequence (5'–3')	Manufacturer
MYH2		Thermo Fisher
Forward	GCAATGTGGAAACGATCTCTAAAGC	
Reverse	GCTGCTGCTCCTCCTCCTG	
Probe	6FAM-TCTGGAGGACCAAGTGAACGAGCTGA-MGBNFQ	
MYH1		
Forward	GGCCCACTTCTCCCTCATTC	
Reverse	CCGACCACCGTCTCATTCA	
Probe	6FAM-CGGGCACTGTGGACTACAACATTACT-MGBNFQ	
PAX7		
Forward	GCCCTCAGTGAGTTCGATTAG	
Reverse	GATGCTGTGCTTGGCTTTC	
Probe	6FAM-TTCGTCCTCCTCCTCCTTCTTCCC-MGBNFQ	

Abbreviations: *MYH1*, myosin heavy chain type IIX; *MYH2*, myosin heavy chain type IIA; *PAX7*, paired box protein 7.

quantitative PCR (qPCR) using diluted total DNA as the template and primers specific to cytochrome c oxidase subunit II (COXII) and actin beta (ACTB) as reference (Li et al., 2009; Guan et al., 2024). Primer and probe sequences (Table 3) were designed from genomic DNA for *COXII* and *ACTB* using Primer Express™ v3.0.1 (Applied Biosystems).

Each qPCR (10 µL total volume) contained 10 ng of genomic DNA template and was run in duplicate on a QuantStudio™ 6 Pro Real-Time PCR System (Applied Biosystems). Thermal cycling conditions consisted of an initial denaturation at 95°C for 20 s, followed by 45 cycles of denaturation at 95°C for 1 s, and annealing/extension at 60°C for 20 s, with fluorescence data collected at the end of each annealing/extension step. The relative mtDNA content was determined using the $2^{-}\Delta Ct$ method, where $\Delta Ct = Ct\ (ACTB) - Ct\ (COXII)$. Thus, mtDNA content represents the ratio of mitochondrial to nuclear DNA abundance within each sample.

Western blotting

For protein extraction, approximately 0.1 g of muscle tissue was homogenized in tissue protein extraction buffer (T-PER™ lysis buffer, Thermo Fisher Scientific) with the addition of a protease inhibitor (Halt™ Protease Inhibitor Cocktail, EDTA-Free, Thermo Fisher Scientific). The total-protein content in the lysates was determined using the bicinchoninic acid assay (Thermo Fisher Scientific) with a NanoDrop™ One/One^{C} Microvolume UV-Vis Spectrophotometer (Thermo Fisher Scientific), measuring the absorbance at 562 nm.

Table 3. TaqMan primer and probe sequences for cytochrome c oxidase subunit II and actin beta used in quantitative polymerase chain reaction quantification of mitochondrial DNA content in semitendinosus muscle.

Gene ID	Gene	Primer and Probe Sequence (5′–3′)	Manufacturer
3283880	COXII		Thermo Fisher
	Forward	6FAM-TCGTCCCGTCCAGGCTTA-MGBNFQ	
	Reverse	6FAM-GTGGTTTGACCCGCAAATTT-MGBNFQ	
	Probe	6FAM-ATTACGGTCAATGCTC-MGBNFQ	
280979	ACTB		
	Forward	6FAM-TCACGGAGCGTGGCTACAG-MGBNFQ	
	Reverse	6FAM-TTGATGTCACGGACGATTTCC-MGBNFQ	
	Probe	6FAM-CACCACCACGGCCGA-MGBNFQ	

Abbreviations: ACTB, actin beta; COXII, cytochrome c oxidase subunit II.

Western blot (WB) analysis was performed using 20 μg of protein denatured at 70°C for 10 min, followed by a second denaturation step at 85°C for 2 min. Denatured protein was loaded onto Bolt 4%–12% Bis-Tris Plus Polyacrylamide Gels (12-well, Thermo Fisher Scientific), underwent gel electrophoresis (200 V for 20 min), and transferred onto polyvinylidene fluoride (PVDF) membranes using the iBlot 2 Dry Blotting System (Thermo Fisher Scientific). To quantify target proteins, the PVDF membranes were stained for total protein using the No-Stain™ Protein Labeling Reagent (Thermo Fisher Scientific) at room temperature for 10 min. The membranes were blocked in a solution containing 3% bovine serum albumin (BSA; Fisher Scientific) and tris-buffered saline with Tween 20 (BIO-RAD Laboratories, Hercules, CA) at room temperature for 30 min. Primary antibodies including anti-HSP27 (mouse monoclonal, dilution 1:1,000; CPTC-HSPB1-1, Developmental Studies Hybridoma Bank [DSHB], Iowa City, IA), anti-HSP60 (rabbit monoclonal, dilution 1:1,000; 12165, Cell Signaling, Danvers, MA, USA), anti-HSP70 (mouse monoclonal, dilution 1:1,000; ab53496, Abcam Inc., Waltham, MA, USA), antiperoxisome proliferator-activated receptor gamma coactivator 1-alpha (PGC-1α; rabbit polyclonal, dilution 1:1000, ab191838, Abcam Inc.), antiperoxisome proliferator-activated receptor alpha (PPARα; rabbit polyclonal, dilution 1:1000, ab126285, Abcam Inc.), anti-PPARγ (rabbit polyclonal, dilution 1:1,000; 2435, Cell Signaling), anti-OXPAT (perilipin 5 [PLIN5]; rabbit polyclonal, dilution 1:1,000; PA1-46215, Invitrogen, Waltham, MA, USA), antisuperoxide dismutase 2 (anti-SOD2; rabbit polyclonal, dilution 1:1,000; PA1-31072, Invitrogen), anti-adenosine monophosphate-activated protein kinase alpha (AMPKα; rabbit polyclonal, dilution 1:1,000; 2532, Cell Signaling), and antiphospho-AMPKα (rabbit monoclonal, dilution 1:1,000; 2535, Cell Signaling), were incubated with the membranes. Secondary antibodies, including goat antimouse IgG (immunoglobulin G) H&L (heavy and light chain) (horseradish peroxidase [HRP]; mouse polyclonal, dilution 1:1,000; ab205719, Abcam Inc.) and goat antirabbit IgG H&L (HRP; rabbit polyclonal, dilution 1:1,000; ab205718, Abcam Inc.), were incubated for 1 h and rinsed following the previously mentioned steps. WB bands were detected using the iBright Imaging System (Applied Biosystems) following the application of 3 mL of SuperSignal West Pico chemiluminescent substrate (Thermo Fisher Scientific). To ensure accurate quantification, protein abundance levels were normalized to total protein, measured using the No-Stain™ Protein Labeling Reagent (Thermo Fisher Scientific). Since multiple samples were analyzed, to account for variation, a reference sample was run on every gel to account for this. Signal intensity was analyzed using the iBright Imaging System software (Applied Biosystems).

Muscle-fiber-type immunohistochemistry

Frozen skeletal muscle samples embedded in optimal cutting temperature compound for immunohistochemistry (IHC) were transferred from −80°C to −20°C and allowed to equilibrate for 24 h. Samples were sectioned at 10-μm thickness in a cross-sectional orientation using a cryostat (CM3050, Leica Biosystems, Buffalo Grove, IL, USA) maintained at −20°C. Sections were mounted on positively charged glass slides (Superfrost; Fisher Scientific, Pittsburgh, PA, USA). For dual immunostaining, 2 slides were prepared from each sample: 1 for paired box protein 7 (PAX7) detection and the other for muscle fiber typing. Five cryosections were placed on each slide, and a hydrophobic barrier was drawn around each section using a PAP Pen (Fisher Scientific).

Tissue fixation was performed in 4% paraformaldehyde prepared in PBS (Thermo Fisher Scientific)

for 10 min at room temperature, followed by 2 PBS rinses. Permeabilization was achieved with 0.25% Triton X-100 in PBS for 10 min and followed by 2 additional rinses. Nonspecific binding was minimized by blocking in 3% BSA (Fisher Scientific) in PBS with Tween 20 (0.1% Tween-20; BIO-RAD) for 30 min at room temperature.

Primary antibodies were diluted in blocking buffer and applied for 1 h at room temperature. For PAX7 staining, sections were incubated with α-dystrophin (rabbit IgG, 1:100; Thermo Fisher Scientific), anti-PAX7 (mouse IgG1, 1:100; DSHB), and 4',6-diamidino-2-phenylindole (DAPI; 1.5 µg/mL; Thermo Fisher Scientific). For muscle fiber typing, antibodies included anti-MyHC-I (BA-D5, mouse IgG2b, 1:100; DSHB) and anti-MyHC-I and -IIA (BF-35, mouse IgG1, 1:100; DSHB). After primary incubation, slides were washed 3 times with PBS and incubated for 1 h in the dark with secondary antibodies diluted in blocking buffer. For PAX7 slides, secondary antibodies included goat antirabbit IgG (H&L) conjugated with Alexa Fluor 594 (1:1,000; Invitrogen) and goat antimouse IgG1 conjugated with Alexa Fluor 488 (1:1,000; Invitrogen). For fiber typing, goat antimouse IgG2b (Alexa Fluor 488, 1:1,000; Invitrogen) and goat antimouse IgG1 (Alexa Fluor 594, 1:1,000; Invitrogen) were used.

Following secondary incubation, slides were rinsed 3 times in PBS and mounted with ProLong Glass Antifade Mountant (Invitrogen) and thin glass coverslips (VWR International, Radnor, PA, USA). Mounted slides were stored at 4°C for 24 h to allow curing. Fluorescence images were acquired using a microscope (EVOS M5000, Thermo Fisher Scientific) at 10× magnification. Five randomly selected fields per slide were analyzed. Total muscle fibers were counted, and fiber types were classified by fluorescence emission: green or yellow fibers as MyHC-I, red fibers as MyHC-IIA, and unstained fibers as MyHC-IIX. ImageJ software (Nation al Institutes of Health, Bethesda, MD, USA) was used to determine the number and proportion of each fiber type relative to the total fiber count.

Statistical analysis

Outcomes measured at both time points (d 0 and d 63) were analyzed using a 2-way analysis of variance (ANOVA) with fixed effects of treatment (IUHS vs. IUCL), time, and their interaction (treatment × time). Outcomes measured at a single time point (d 63) were analyzed using an unpaired *t* test with Welch's correction. The individual calf served as the experimental unit for all outcomes. For gene expression and mtDNA abundance, technical qPCR replicates were averaged to obtain a single value per calf before statistical analysis. For IHC, 5 fields per slide were quantified and averaged to obtain a single value per calf before statistical analysis. Since distinct calves were sampled at each time point, observations were independent across time; therefore, a repeated-measures framework was not applicable. Outcomes were analyzed using a 2-way ANOVA with fixed effects of treatment, time, and their interaction with the individual calf as the experimental unit. Analyses were conducted using GraphPad Prism (version 9.4.1; GraphPad Software, San Diego, CA, USA). The relative abundance of phosphorylated AMPK was also expressed as a ratio to total AMPK ($R = \frac{pAMPK}{AMPK}$) and analyzed under the same factorial model. When the interaction was significant ($P < .05$), Tukey's honestly significant difference procedure was used for pairwise comparisons among the 4 cell means while controlling the familywise error rate. Results are reported as mean ± standard error of the mean (SEM). Statistical significance was declared at a P value of less than .05. A P value between .05 and .10 was interpreted as a statistical tendency. Exact P values are provided unless P was less than .01, in which case the result is reported as "$P < .01$" for readability.

Results

Gene expression

Gene expression is presented in Table 4. A significant treatment × time interaction was observed for *HSP27* ($P = .042$). *HSP27* transcript abundance did not differ between treatments at d 0 but was higher in IUHS than IUCL at d 63, indicating a larger treatment difference at d 63. No treatment × time interaction was detected for *HSP60* ($P = .454$), and IUHS dairy heifers exhibited greater *HSP60* mRNA abundance compared with IUCL across both time points ($P = .001$). *HSP70* expression showed no interaction ($P = 0.205$) or time effect ($P = .242$), although there was a tendency for higher expression in IUHS dairy heifers ($P = .100$). A significant treatment × time interaction was detected for *ATF4* ($P = .003$). Breaking down this interaction, IUHS dairy heifers exhibited minimal expression change from d 0 to d 63 compared with their IUCL counterparts, which showed an increase from d 0 to d 63 driving this interaction. No treatment × time interactions were detected for *PAX7* ($P = .154$), *insulin-like growth factor 1* (*IGF-1*; $P = .826$), or *myogenic factor 5* (*Myf5*; $P = .794$).

Table 4. Effects of in utero heat stress on relative messenger RNA expression of heat-shock, myogenic, and metabolic genes in semitendinosus muscle of heifer calves at birth (day 0) and postweaning (day 63).

Genes	Day	IUCL	IUHS	Temp	Time	T × T
HSP27	0	1.56 ± 0.32[b]	2.52 ± 0.29[b]	0.001	<0.001	0.042
	63	2.55 ± 0.4[b]	5.83 ± 0.92[a]			
HSP60	0	0.97 ± 0.21	2.00 ± 0.20	0.001	0.492	0.454
	63	0.94 ± 0.27	2.54 ± 0.63			
HSP70	0	4.86 ± 1.76	12.82 ± 2.77	0.100	0.242	0.205
	63	11.48 ± 2.68	12.55 ± 3.21			
ATF4	0	0.96 ± 0.13[b]	1.66 ± 0.12[ab]	0.705	0.002	0.003
	63	2.58 ± 0.4[a]	1.70 ± 0.20[ab]			
PAX7	0	0.57 ± 0.12	1.33 ± 0.32	0.187	<0.001	0.154
	63	2.41 ± 0.34	2.38 ± 0.25			
IGF-1	0	0.76 ± 0.07	0.64 ± 0.08	0.400	<0.001	0.826
	63	1.55 ± 0.30	1.35 ± 0.20			
Myf5	0	1.09 ± 0.23	1.30 ± 0.14	0.761	0.002	0.794
	63	2.45 ± 0.36	2.47 ± 0.71			
MyoD	0	3.17 ± 0.64[b]	4.23 ± 0.6[b]	0.008	0.005	0.087
	63	4.42 ± 0.75[b]	8.99 ± 1.55[a]			
MyoG	0	2.36 ± 0.68[b]	3.59 ± 0.48[b]	0.001	0.002	0.068
	63	3.44 ± 0.62[b]	7.38 ± 1.03[a]			
MYH7	0	3.37 ± 2.19	4.37 ± 1.26	0.132	0.148	0.300
	63	4.24 ± 1.00	9.50 ± 2.85			
MYH2	0	1.36 ± 0.15[b]	3.32 ± 0.19[a]	0.539	0.002	0.002
	63	4.66 ± 0.63[a]	3.29 ± 0.66[a]			
MYH1	0	1.61 ± 0.40	4.26 ± 0.29	<0.001	0.937	0.753
	63	1.75 ± 0.27	4.02 ± 0.96			
C/EBPα	0	2.87 ± 1.09	12.93 ± 3.33	0.006	0.592	0.500
	63	3.25 ± 0.93	9.65 ± 3.53			
PPARα	0	1.18 ± 0.15	3.41 ± 0.27	0.003	0.002	0.338
	63	3.71 ± 0.89	7.90 ± 1.77			
PPARγ	0	0.86 ± 0.18	1.18 ± 0.10	0.673	0.002	0.930
	63	3.14 ± 0.84	3.35 ± 1.30			
PGC-1α	0	4.27 ± 1.37	6.58 ± 2.66	0.145	0.003	0.349
	63	13.95 ± 3.94	24.25 ± 7.34			
PLIN5	0	1.75 ± 0.48	6.13 ± 0.90	0.023	<0.001	0.264
	63	8.57 ± 1.65	10.14 ± 1.91			

Abbreviations: ANOVA, analysis of variance; ATF4, activating transcription factor 4; HMBS, hydroxymethylbilane synthase; HSP, heat-shock protein; day 0, d 0; day 63, d 63; IGF-1, insulin-like growth factor 1; IUCL, in utero cooled; IUHS, in utero heat stressed; LSMeans, least-squares means; Myf5, myogenic factor 5; MyoD, myoblast determination protein 1; MyoG, myogenin; PGC-1α, peroxisome proliferator-activated receptor gamma coactivator 1-alpha; PLIN5, perilipin 5; PPAR, peroxisome proliferator-activated receptor; RPS9, ribosomal protein subunit 9; SEM, standard error of the mean; temp, temperature.

Values represent relative expression (LSMeans ± SEM) normalized to the geometric mean of RPS9 and HMBS reference genes. Statistical effects were determined by 2-way ANOVA with fixed effects of temperature (IUCL, IUHS), time (d 0 and 63), and their interaction (treatment × time). $P < .05$ was considered significant. Different letters denote $P < .05$ among the 4 treatment × time LSMeans (Tukey's multiple comparisons test).

For each of these genes, transcript abundance increased from d 0 to d 63 (*PAX7* and *IGF-1*, $P < 0.001$; *Myf5*, $P = .002$) without an overall treatment effect (*PAX7*, $P = .187$; *IGF-1*, $P = .367$; *Myf5*, $P = .535$). A tendency for a treatment × time interaction was observed for *myoblast determination protein 1* (*MyoD*; $P = .087$) and *myogenin* (*MyoG*; $P = .068$). For both genes, transcript abundance increased over time (*MyoD*, $P = .005$; *MyoG*, $P = .002$) and was greater in IUHS than IUCL (*MyoD*, $P = .008$; *MyoG*, $P = .001$), and the IUHS vs. IUCL difference was numerically larger at d 63 than at d 0.

No treatment × time interaction was detected for *MYH7* ($P = .300$), and neither the treatment ($P = .132$) nor the time effects ($P = .148$) were significant. A significant treatment × time interaction was observed for *MYH2* transcript abundance ($P = .002$). In IUCL, *MYH2* transcript abundance increased from d 0 to d 63, whereas *MYH2* expression changed little over time in IUHS, resulting in convergence of treatment means by d 63, with greater *MYH2* abundance in IUHS than IUCL at d 0. *MYH1* transcript abundance was greater in IUHS than IUCL ($P < .001$), with no time effect ($P = .937$) and no treatment × time interaction ($P = .753$).

No treatment × time interaction was detected for *CCAAT/enhancer-binding protein alpha* ($P = .500$), and expression was greater in IUHS than IUCL across time points ($P = .006$) with no time effect ($P = .592$). *PPARα* showed no interaction ($P = .338$) but was greater in IUHS than IUCL ($P = .003$) and increased over time ($P = .002$). For *PPARγ* and *PGC-1α*, no treatment effect and no interaction were detected (*PPARγ* treatment $P = .673$ and interaction $P = .930$; *PGC-1α* treatment $P = .145$ and interaction $P = .349$), although both increased from d 0 to d 63 (*PPARγ*, $P = .002$; *PGC-1α*, $P = .003$). Finally, *PLIN5* showed no interaction ($P = .264$) but was greater in IUHS than IUCL ($P = .023$) and increased over time ($P < .001$).

Protein abundance

Protein abundance is presented in Figure 1. HSP27 protein abundance exhibited a treatment × time interaction ($P = .001$; Figure 1A), with similar levels between groups at d 0 but lower abundance in IUHS than IUCL at d 63. HSP60 showed a tendency for a treatment × time interaction ($P = .053$; Figure 1B). IUHS was higher at d 0; however, abundance declined in both groups by d 63, and the difference between treatments was reduced. HSP70 protein abundance exhibited a treatment × time interaction ($P < .001$; Figure 1C). HSP70 protein levels did not differ between IUHS

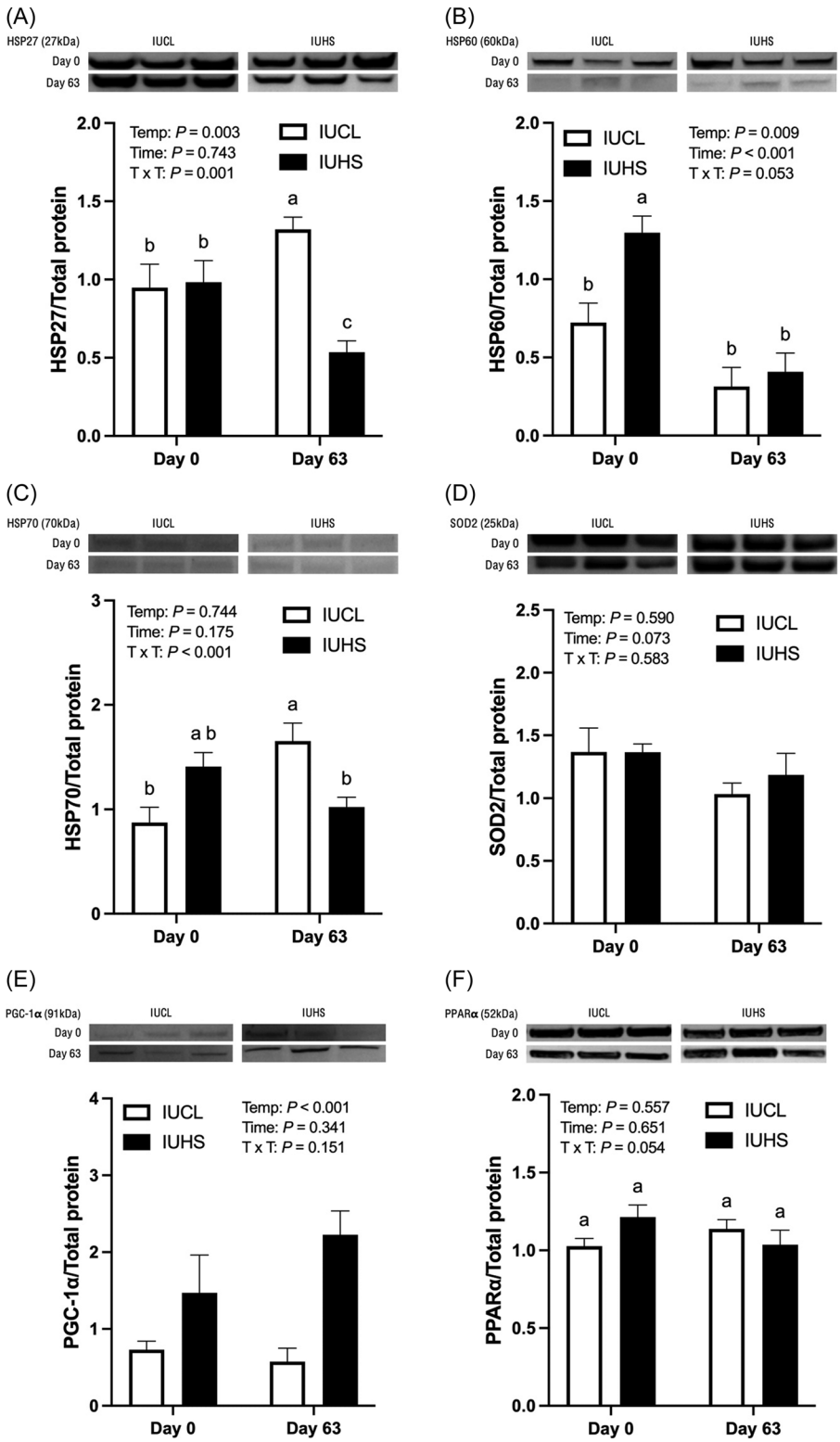

Figure 1. Effects of inutero heat stress on protein abundance of stress and metabolic regulators in semitendinosus muscle at birth (day 0) and postweaning (day 63). Representative immunoblots and quantified protein abundance (mean ± SEM) normalized to total protein are shown for: (A) HSP27, (B) HSP60, (C) HSP70, (D) SOD2, (E) PGC-1α, (F) PPARα, (G) PPARγ, (H) PLIN5, (I) AMPK, (J) p-AMPK, and (K) p-AMPK:AMPK ratio in heifer calves from the IUCL (open bars) or IUHS (filled bars) dams. Protein signals were quantified from WB and normalized with total-protein staining. Statistical effects were tested by 2-way ANOVA with fixed effects of temperature (IUCL vs. IUHS), time (d 0 vs. d 63), and the temperature × time interaction. Different letters denote $P < .05$ among the 4 temperature × time means (Tukey's test). Abbreviations: AMPK; adenosine monophosphate-activated protein kinase; ANOVA, analysis of variance; day 0, d 0; day 63, d 63; HSP, heat-shock protein; IUCL, in utero cooled; IUHS, in utero heat stressed; p-AMPK, phosphorylated AMPK; PGC-1α, peroxisome proliferator-activated receptor gamma coactivator 1-alpha; PLIN5, perilipin 5; PPAR, peroxisome proliferator-activated receptor; SEM, standard error of the mean; SOD2, superoxide dismutase 2; temp, temperature; WB, Western blot.

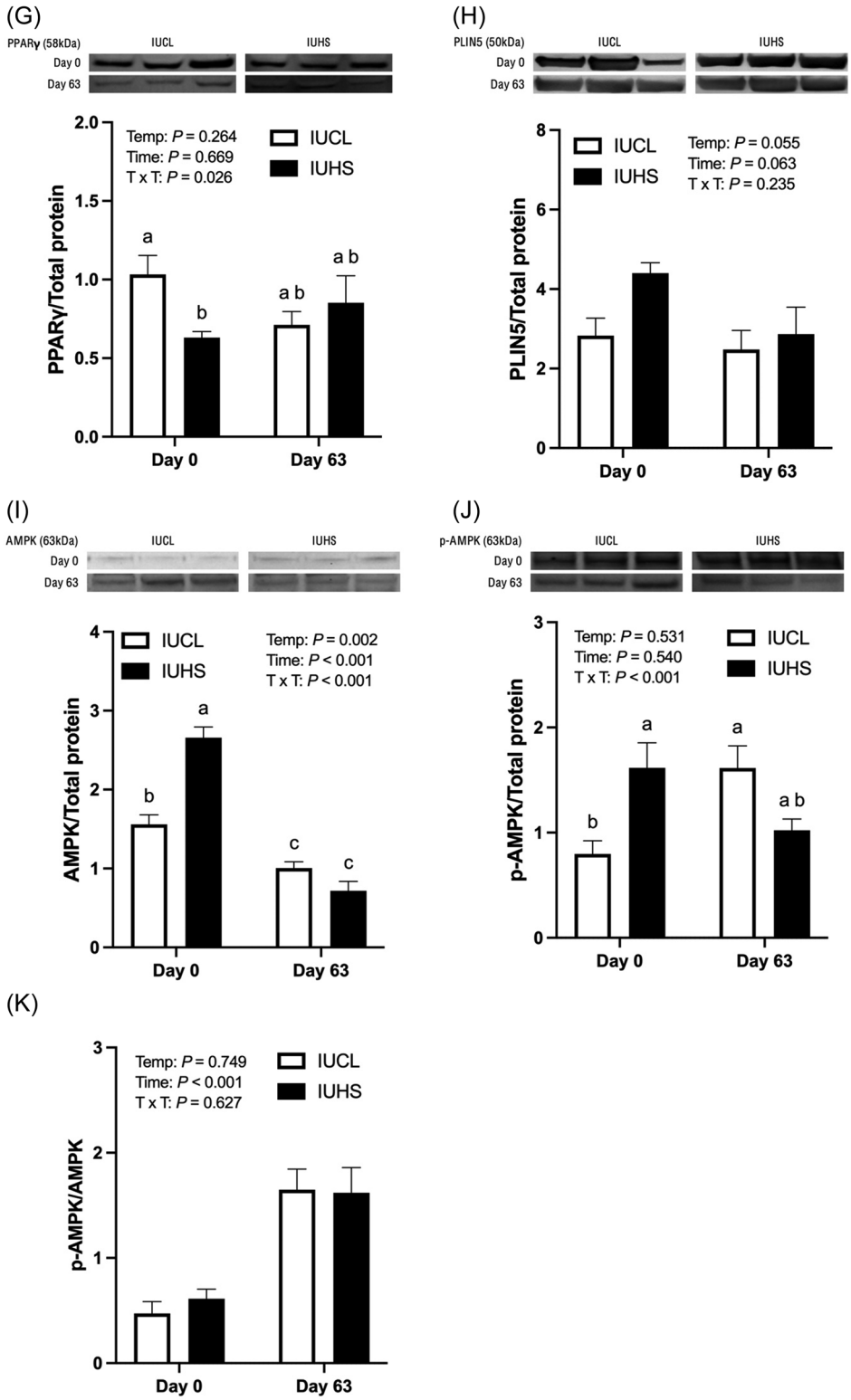

Figure 1. (*Continued*)

and IUCL at birth (d 0), whereas IUHS heifers exhibited lower HSP70 protein abundance than IUCL heifers at d 63. SOD2 abundance was not affected by treatment, time, or their interaction ($P = .590$, $P = .073$, and $P = .583$, respectively; Figure 1D). PGC-1α showed no treatment × time interaction ($P = .151$) and no time effect ($P = .341$), but abundance was greater in IUHS than IUCL ($P < .001$; Figure 1E). PPARα showed a tendency for a treatment × time interaction ($P = .054$; Figure 1F). PPARγ exhibited a

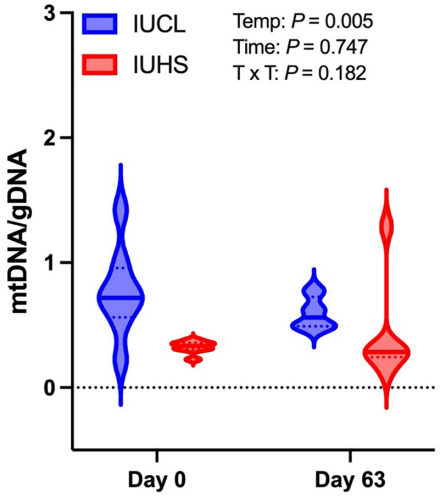

Figure 2. Relative mitochondrial DNA to genomic DNA ratio in semitendinosus muscle of in utero cooled and heat-stressed heifers at birth (day 0) and day 63. Values are shown as violin plots with median (solid line) and interquartile range (dashed lines). Statistical effects were evaluated by 2-way ANOVA. No temperature × time interaction was detected, and the figure reflects the main effect of in utero treatment. Abbreviations: ANOVA, analysis of variance; gDNA, genomic DNA; IUCL, in utero cooled; IUHS, in utero heat stressed; mtDNA, mitochondrial DNA; temp, temperature.

treatment × time interaction ($P = .026$; Figure 1G), indicating that the pattern of change over time differed between treatments. PLIN5 showed no treatment × time interaction ($P = .235$), although tendencies for treatment and time effects were observed (Figure 1H). Total AMPK abundance exhibited a treatment × time interaction ($P < .001$; Figure 1I), with higher AMPK in IUHS at d 0, followed by declines in both groups by d 63. Phospho-AMPK also showed a treatment × time interaction ($P < .001$; Figure 1J), indicating that the treatment difference changed over time. The ratio of phospho-AMPK to total AMPK increased from d 0 to d 63 ($P < .001$) and was not affected by treatment or their interaction (Figure 1K).

Mitochondrial abundance

No treatment × time interaction was detected for mtDNA content ($P = .182$), and no main effect of time was observed ($P = .747$). Across time points, IUHS calves had lower mtDNA content than IUCL calves ($P = .005$; Figure 2).

Satellite-cell abundance and fiber-type composition

Muscle cross-sections from calves exposed to IUHS contained a greater number of $PAX7^+$ cells compared with those from the IUCL group (11.50 vs. 8.55; $P = .005$; Figure 3). The proportion of type I fibers (MyHC-I) was higher in IUHS muscle than in IUCL (23.99% vs. 21.41%; $P = .020$). Conversely, IUHS dairy heifers exhibited a lower proportion of type IIA fibers (23.37% vs. 31.31%; $P < .001$) and a higher proportion of type IIX fibers (52.64% vs. 47.28%; $P = .027$; Figure 4).

Discussion

Dairy heifers exposed to IUHS were born earlier (approximately 3 d before) than those from cooled dams and had a significantly lower birth weight (approximately 4 kg lighter). The impact of IUHS extended throughout the preweaning period, with these dairy heifers exhibiting a 7% reduction in average daily gain compared to the IUCL group, leading to consistently lower body weights and reduced starter intake (Dado-Senn et al., 2021). Additionally, their growth trajectory was impaired, as evidenced by smaller body measurements, including hip height, withers height, body length, chest girth, waist girth, and head circumference, which remained reduced through d 56. Using the same cohort of animals, IUHS dairy heifers exhibited a reduced mammary gland length at d 0 and d 63, along with lighter mammary parenchyma and fat pad mass (Dado-Senn et al., 2022).

Despite the overall decline in body growth and mammary gland development, the dissected ST muscle weight was similar between in the IUHS and control dairy heifers at d 0 and d 63. Likewise, muscle weight relative to body weight showed no significant differences at either time point, indicating that IUHS did not selectively impair skeletal muscle development. However, our findings indicate that in utero hyperthermia induced distinct transcriptional and translational responses in skeletal muscle, revealing significant molecular adaptations to HS during fetal development.

The ST muscle exhibits marked regional heterogeneity with distinct oxidative and glycolytic zones. Samples were collected from a standardized midbelly, central internal region to minimize within-muscle variability. The present results should be interpreted as most representative of this mixed region and may not fully reflect responses in the more extreme superficial glycolytic or deep oxidative portions.

Stress resilience and molecular adaptations in metabolism growth and skeletal muscle development

At d 0, IUHS dairy heifers exhibited higher transcript abundance of *HSP60* than IUCL, whereas

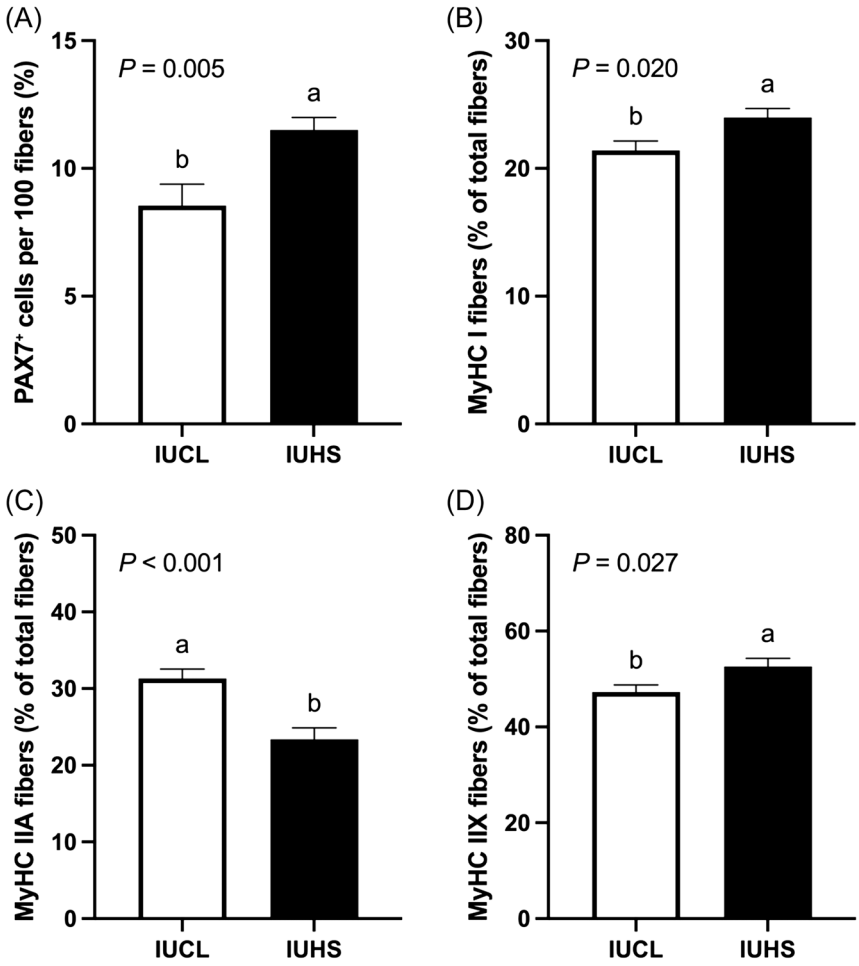

Figure 3. Satellite-cell abundance and muscle-fiber-type composition in semitendinosus muscle of heifer calves exposed to in utero heat stress or cooling evaluated at day 63. (A) PAX7$^+$ cells per 100 fibers; (B) type I (MyHC-I); (C) type IIA (MyHC-IIA); and (D) type IIX (MyHC-IIX) fibers expressed as a percentage of total fibers. Data are mean ± SEM ($n = 8$/group). Statistical differences between IUCL (open bars) and IUHS (filled bars) were determined by unpaired *t* test with Welch's correction. Different letters (a, b) indicate $P < .05$. IUHS heifers had more PAX7$^+$ cells and a higher proportion of type I and IIX fibers but fewer type IIA fibers than IUCL heifers. Abbreviations: IUCL, in utero cooled; IUHS, in utero heat stressed; MyHC, myosin heavy chain; PAX7, paired box protein 7; SEM, standard error of the mean.

HSP70 mRNA did not differ between treatments and only tended to be higher in IUHS. Importantly, *HSP27* showed a treatment × time interaction, with no treatment difference at d 0 but greater abundance in IUHS at d 63, indicating a larger separation with age. In contrast, *HSP60* mRNA showed no interaction and remained greater in IUHS than IUCL across time points.

At the protein level, temporal responses differed among each kind of HSP. HSP27 protein exhibited a treatment × time interaction, with similar abundance at d 0, but lower abundance in IUHS than IUCL at d 63. HSP60 protein showed a tendency for a treatment × time interaction, which was higher in IUHS at d 0 followed by a decline in both groups by d 63 that reduced the between-treatment difference. HSP70 protein abundance exhibited a significant treatment × time interaction, with no difference between IUHS and IUCL at birth (d 0) but lower abundance in IUHS dairy heifers at d 63. This pattern indicates that prenatal heat exposure altered the postnatal regulation of the heat-shock response in skeletal muscle rather than inducing a persistent elevation at birth. Because animal handling and tissue collection procedures were standardized across treatments, the observed difference at d 63 is unlikely to reflect acute handling stress. Instead, these results are most consistent with age-dependent modulation of HSP70 protein abundance following prenatal heat exposure. Stress responsiveness, including hypothalamic–pituitary–adrenal axis activity, was not directly assessed in the present study and therefore cannot be inferred from HSP70 protein abundance alone.

The role of HSPs in skeletal muscle growth is still ambiguous, but there are a few possible mechanisms that may directly or indirectly impact skeletal muscle growth. During the muscle regeneration process, Types of HSP, particularly HSP70, are thought to play a critical

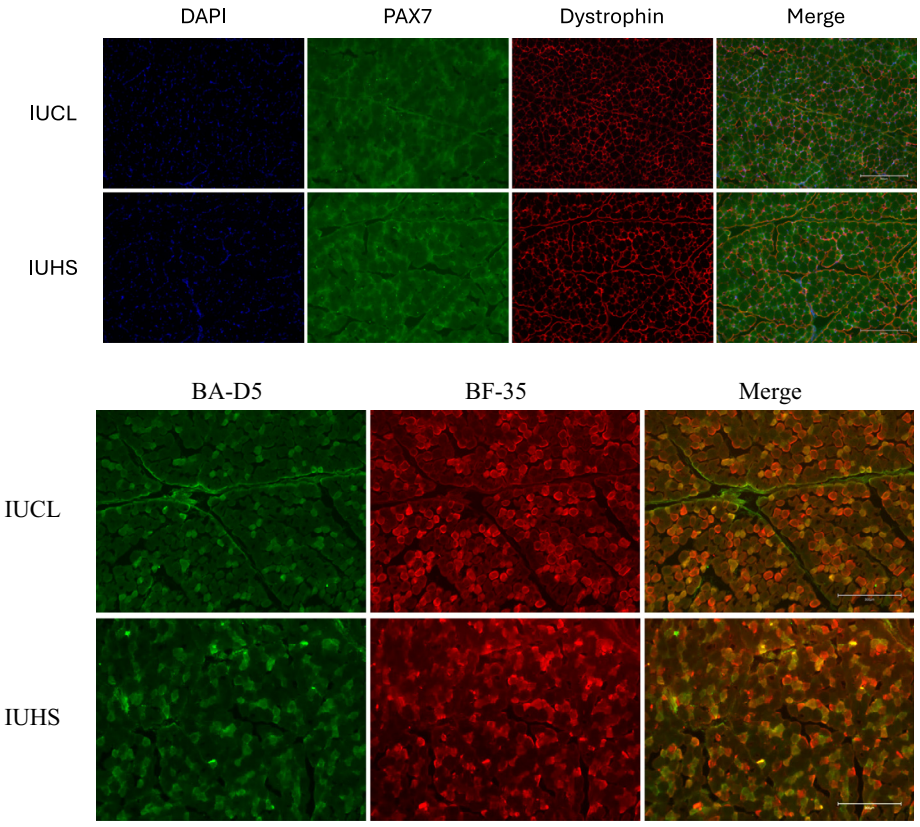

Figure 4. Representative immunofluorescence images showing myosin heavy chain fiber-type distribution and PAX7^{+} satellite cells in semitendinosus muscle of heifer calves exposed to in utero cooling or in utero heat stress. (Top panels) Sections stained with BA-D5 (MyHC-I, green) and BF-35 (MyHC-I and IIA, but not IIX, red) antibodies illustrate fiber-type composition, and merged images show MyHC-I fibers in green, MyHC-IIA fibers in red, and MyHC-IIX fibers unstained. (Bottom panels) Sections stained with DAPI (nuclei, blue), PAX7 (green), and dystrophin (red) display PAX7^{+} nuclei positioned beneath the dystrophin-labeled sarcolemma. All images were captured at 10× magnification. Scale bar = 300 µm. Abbreviations: DAPI, 4',6-diamidino-2-phenylindole; IUCL, in utero cooled; IUHS, in utero heat stressed; MyHC, myosin heavy chain; PAX7, paired box protein 7.

role in promoting muscle fiber regeneration by modulating the Forkhead box O (FoxO) and nuclear factor kappa-light-chain-enhancer of activated B cells signaling pathways and regulating the immune response to facilitate efficient tissue repair (Moresi et al., 2009; Senf et al., 2013). In our previous study, we found evidence that HSP27 can directly bind to an MRF and Myf5 and potentially regulate the heterogeneous population of satellite cells, interfering with determining whether cells proceed to the myogenic regulation or proliferation stage (Kim et al., 2023). However, the direct role of HSPs in postnatal skeletal muscle growth remains largely unexplored and requires further investigation.

Metabolic adaptations to in utero heat stress: shifts toward oxidative pathways and lipid utilization

Another possible mechanism by which HSPs contribute to mitochondrial biogenesis involves HSP60. HSP60 is a mitochondrial chaperone that, together with its cochaperonin, HSP10, facilitates the proper folding and assembly of newly synthesized mitochondrial proteins (Barone et al., 2016). It plays a critical role in maintaining protein homeostasis, preventing the aggregation of misfolded proteins, and ensuring optimal mitochondrial function. Additionally, HSP60 has been implicated in coordinating with PGC-1α, a key regulator of mitochondrial biogenesis and oxidative metabolism (Marino Gammazza et al., 2018). Our current data from d 63 heifers indicate an increase in *PGC-1α* mRNA and a 3.8-fold increase in PGC-1α protein levels in skeletal muscle, which correlated with increased *HSP60* expression. PGC-1α is known to interact with multiple nuclear transcription factors, including members of the PPAR family, nuclear respiratory factors (NRF-1 and NRF-2), estrogen-related receptor alpha, myocyte enhancer factor-2, FoxO 1, and sterol regulatory element-binding protein 1 (Knutti and Kralli, 2001; Kang and Ji, 2012). The connection between PGC-1α and HS in skeletal muscle remains uncertain. However, PGC-1α likely helps

reduce oxidative stress, as PGC-1α knockout mice show increased vulnerability to oxidative damage (St-Pierre et al., 2006). The increased expression of *PGC-1α*, along with higher HSP60 levels, suggests that skeletal muscle may be shifting its energy metabolism toward oxidative pathways, a pattern observed in previous studies on how muscles adapt to temperature stress (Hafen et al., 2018; Kim and Kim, 2023; Smith et al., 2023).

In IUHS calves, a reduction in the mtDNA to genomic DNA (gDNA) ratio was observed, indicating lower mtDNA copy number relative to nuclear DNA and potentially reflecting altered mitochondrial density or remodeling. Although the mtDNA to gDNA ratio is commonly used as a proxy for mitochondrial abundance, this measure assumes comparable nuclear DNA content per unit tissue and similar cellular composition across treatments. Therefore, differences in the mtDNA to gDNA ratio may also be influenced by variation in nuclear density or contributions of non-myofiber cell populations and should be interpreted as a relative index rather than a direct measure of absolute mitochondrial abundance in muscle tissue. Even with these limitations, reduced mtDNA relative to gDNA can be consistent with constrained mitochondrial proliferation or a remodeling process. In mammalian systems, depletion or dysfunction of mtDNA engages the mitochondrial unfolded-protein response (UPR^{mt}), which upregulates mitochondrial chaperones such as HSP60 and HSP10 to restore proteostasis (Muñoz-Carvajal and Sanhueza, 2020; Keerthiga et al., 2021). Concurrently, energetic stress typically activates the AMPK-PGC-1α axis in skeletal muscle, thereby initiating compensatory mitochondrial biogenesis programs (Jäger et al., 2007; Abu Shelbayeh et al., 2023). Overall, the combination of lower mtDNA content with higher HSP60 and increased PGC-1α is consistent with a compensatory response, potential UPR^{mt}-driven chaperone induction, and PGC-1α-mediated biogenesis signaling to mitigate prenatal HS-induced mitochondrial insufficiency. ATF4 transcript abundance exhibited a significant treatment × time interaction, reflecting divergent temporal patterns between treatments. ATF4 expression increased from birth to postweaning in IUCL heifers, whereas IUHS heifers maintained relatively stable, intermediate ATF4 expression across time points. These findings indicate that prenatal heat exposure modified the developmental regulation of ATF4 expression rather than inducing consistent activation or suppression at specific time points. Because ATF4 participates in multiple stress-responsive pathways, including the integrated stress response and endoplasmic reticulum stress, direct functional or mechanistic implications cannot be inferred from transcript abundance alone.

Phosphorylated AMPK showed a significant temperature × time interaction, characterized by higher p-AMPK levels in IUHS calves at birth with convergence between groups by d 63. This pattern is consistent with a transient early difference in cellular energy sensing rather than a persistent treatment effect across development. In contrast, transcripts involved in lipid handling and oxidative metabolism increased with age in both groups. *PPARα* and *PLIN5* mRNA were higher in IUHS overall and increased from birth to d 63, indicating strong developmental regulation with an additional treatment shift. At d 63, PPARα protein abundance and PLIN5 protein levels did not differ between treatments, suggesting that transcriptional differences did not translate into detectable differences at the protein level at this time point. Functionally, PPARα regulates genes involved in fatty-acid uptake and oxidation in skeletal muscle, and PLIN5 supports intramyocellular lipid storage and mobilization, with evidence that increased PLIN5 can promote fatty-acid breakdown and mitochondrial oxidation (Bosma et al., 2013). SOD2 abundance did not differ between groups, suggesting that oxidative stress levels were not high enough to induce a mitochondrial antioxidant response. *ATF4* gene expression was reduced at d 0 and showed a decreasing trend at d 63, consistent with limited activation of ATF4-mediated antioxidant pathways.

Mitochondrial remodeling and oxidative fiber adaptation under prenatal heat stress

The concurrent decrease in mtDNA abundance and the shift in type I (MyHC-I) fiber proportion in IUHS heifers suggest a potential alteration in the cellular metabolic environment. Although mtDNA copy number is often used as a proxy for mitochondrial content, mitochondrial function is also shaped by turnover, proteostasis, and transcriptional reprogramming (Kang and Ji, 2012). The reduced mtDNA content observed in IUHS muscle indicates limited mitochondrial proliferation, yet increased *HSP60*, *PGC-1α*, and *PPARα* expression suggest activation of compensatory pathways consistent with mitochondrial remodeling and altered metabolic regulation; however, direct functional assays are needed to confirm changes in oxidative capacity or efficiency. In IUHS dairy heifers, the overall elevation in *HSP60* mRNA (encoding a mitochondrial chaperone essential for protein import and folding) may be consistent with altered regulation of mitochondrial

proteostasis pathways, including the UPR^{mt}, which maintains protein quality by inducing HSP60 and HSP10 (Muñoz-Carvajal and Sanhueza, 2020). UPR^{mt} activation can coordinate with PGC-1α to promote mitochondrial repair and biogenesis (Barone et al., 2016; Marino Gammazza et al., 2018), suggesting that the elevated PGC-1α protein represents a compensatory response to prenatal stress-induced mitochondrial insufficiency rather than an expansion of mitochondrial mass. Similar adaptations have been reported in heat-acclimated human muscle, where oxidative capacity increases without a parallel rise in mtDNA content (Hafen et al., 2018). The higher proportion of type I fibers in IUHS muscle, together with a higher proportion of type IIX fibers and a lower proportion of type IIA fibers, suggests prenatal HS altered postnatal fiber-type remodeling rather than producing a uniform shift toward a single phenotype. The increase in type I fibers is consistent with oxidative programming and may align with AMPK activation and enhanced PGC-1α signaling, which promotes oxidative gene expression. At the same time, the concurrent enrichment of type IIX fibers may indicate altered maturation of fast-fiber subtypes, with a relative depletion of the intermediate type IIA population. Functionally, this mixed fiber-type pattern could influence metabolic flexibility and growth performance by shifting the balance between oxidative capacity and fast contractile characteristics. Consistent with this interpretation, AMPK activation, observed as higher AMPK and phosphorylated AMPK at birth, can enhance PGC-1α activity, stimulating oxidative gene expression and promoting a slow-oxidative phenotype (Knutti and Kralli, 2001; Jäger et al., 2007). This mechanism aligns with reports that metabolic remodeling can precede shifts in myosin isoform composition under chronic energetic stress (Pereyra et al., 2022). The concurrent increase in *MyoD* and *MyoG* expression at d 63 further supports postnatal activation of satellite cells and continued differentiation toward oxidative myogenesis (Kim and Kim, 2023). Although mtDNA content was reduced, IUHS dairy heifers maintained skeletal muscle weight relative to body weight. This implies that prenatal HS may have driven compensatory mitochondrial remodeling, such as altered turnover and quality-control processes, allowing maintenance of muscle mass despite reduced mtDNA content. The concurrent elevation of *HSP60* mRNA and PGC-1α expression is consistent with enhanced coordination of mitochondrial proteostasis and biogenesis signaling, which may support mitochondrial turnover and remodeling (St-Pierre et al., 2006). This pattern resembles the improved mitochondrial efficiency reported in heat-acclimated skeletal muscle (Hafen et al., 2018). Reduced mtDNA abundance despite elevated PGC-1α may also reflect suppression of mitochondrial transcription factor A, a regulator required for mtDNA replication and stability (Kuo et al., 2013). Such inhibition under stress conditions would limit mitochondrial proliferation even in the presence of biogenic signaling.

In utero heat stress on myogenic regulation and skeletal muscle adaptation

At d 0, no differences were detected in the mRNA expression levels of key MRF types, including *Myf5*, *MyoD*, and *MyoG*, between the muscle of IUHS and IUCL dairy heifers. However, post hoc pairwise comparisons indicated that the treatment difference for *MyoD* and *MyoG* were not evident at d 0 but were significant by d 63, with higher expression in IUHS than IUCL at d 63. These findings suggest that prenatal HS did not markedly alter the transcriptional regulation of early myogenic differentiation at birth, but differences in myogenic regulatory programs became evident during postnatal development. In contrast, MyHC isoform transcript analysis indicated a significant overall treatment effect for *MYH1* and a significant treatment × time interaction for *MYH2*. For *MYH2*, this interaction reflected differences in temporal regulation rather than opposing treatment effects at each time point. Specifically, *MYH2* expression increased with age in IUCL dairy heifers, whereas IUHS dairy heifers showed relatively stable expression across time, leading to similar *MYH2* abundance between treatments by d 63. These findings indicate that prenatal heat exposure altered the developmental trajectory of *MYH2* expression without producing a sustained treatment difference at the postweaning time point. Consequently, functional implications related to fast-fiber subtype transitions should be interpreted cautiously. As a master regulator of myogenic commitment, *MyoD* initiates the transcription of other MRF and muscle-specific genes required for myofiber formation (Hernández-Hernández et al., 2017). *MyoG*, although also required for differentiation, plays a more progressive role by regulating the transcription of structural proteins (Zammit, 2017). In the previous study, bovine myocytes exposed to 41°C for 48 h showed elevated *MyoD*, *MyoG*, and *IGF-1* expression compared with thermoneutral cells, resulting in a greater differentiation index, increased myotube diameter, and higher protein synthesis rate

(Kim and Kim, 2023). Similar responses have been observed in beef cattle exposed to thermal fluctuations, further supporting temperature-driven modulation of myogenic signaling (Smith et al., 2023). Under moderate rather than severe heat conditions, thermal cues may stimulate satellite-cell activity and promote hypertrophic adaptation without impairing immune function (Halevy et al., 2001; Xu et al., 2022). Evidence across species remains mixed, but in general, mild, or transient HS tends to enhance myogenesis through MRF upregulation and anabolic signaling, whereas prolonged or extreme stress suppresses proliferation and favors adipogenic conversion (Piestun et al., 2017; Johnson et al., 2020).

The higher number of PAX7$^+$ cells in IUHS muscle, together with the postnatal increase in *MyoD* and *MyoG* transcripts at d 63, indicates coordinated activation of the myogenic lineage following prenatal heat exposure. Within the myogenic lineage, satellite cells marked by PAX7 undergo MyoD-dependent activation and MyoG-guided differentiation, coordinating progenitor preservation with myofiber formation (Olguín and Pisconti, 2012; Hernández-Hernández et al., 2017). Although *PAX7* mRNA did not differ statistically between treatments, IHC revealed greater PAX7$^+$ cell abundance, consistent with cellular heterogeneity diluting transcript differences in whole tissue. The concurrent rise in *MyoD* and *MyoG* expression suggests that IUHS both expanded and primed the satellite-cell pool for differentiation during early postnatal growth. Mechanistically, the coordinated increase in PAX7$^+$ cells and MRF expression may reflect the activation of stress-responsive signaling networks that integrate environmental cues with myogenic regulation. Moderate heat exposure is known to enhance satellite-cell activation and proliferation through HSP-mediated modulation of Myf5 and downstream mitogen-activated protein kinase-p38 signaling, which promote myoblast commitment and differentiation (Halevy et al., 2001; Xu et al., 2022). In parallel, AMPK-mTOR and IGF-1-Akt pathways act as central metabolic checkpoints that facilitate energy-dependent myogenic progression, supporting both protein synthesis and myotube hypertrophy under sublethal thermal stress (Uehara et al., 2004; Ma et al., 2018; Fennel et al., 2023). Evidence from several species indicates that moderate heat exposure can enhance myogenesis by coupling cellular energy sensing with the activation of MRF. Such responses appear to promote satellite-cell proliferation and differentiation while maintaining the pool of progenitor cells.

Potential mechanisms and long-term implications of in utero heat stress on skeletal muscle development

The observed postnatal increases in *MyoD* and *MyoG* expression, along with changes in fiber phenotype, raise the question of whether these responses represent transient adaptations or long-term reprogramming of muscle growth and metabolism. The long-term effects of IUHS on skeletal muscle development remain complex and potentially contradictory, requiring further investigation. One possibility is that early-life exposure to HS activates inflammatory pathways or autophagic cellular processes, as recently observed in the liver tissue by Laporta et al. (2025), which may share mechanistic parallels with skeletal muscle adaptation to thermal stress. The upregulation of inflammatory cytokines in response to IUHS could induce systemic immune activation, leading to muscle damage while simultaneously enhancing transcriptional programs associated with muscle regeneration and hypertrophy. Alternatively, HS may serve as an anabolic stimulus for skeletal muscle growth and metabolism, particularly under moderate conditions. However, defining the threshold at which HS shifts from a compensatory to a detrimental factor remains critical.

The companion study by Dado-Senn et al. (2021) suggested that IUHS impacts survival and productivity for multiple years and lactations. Skibiel et al. (2018) found 135 differentially methylated genes in the mammary gland of first lactation IUHS dairy heifers. By analogy, our findings of prolonged upregulation of stress-related genes and proteins in skeletal muscle, including HSP60 and MRF, suggest that similar epigenetic modifications could underlie persistent molecular phenotypes in muscle tissue. It is also notable that some stress markers (e.g., HSP70) may reflect transient responses, highlighting the need to distinguish between enduring molecular imprints and acute stress effects.

Future research should focus on assessing epigenetic modifications in stress-responsive genes, including those involved in proteostasis, mitochondrial biogenesis, and myogenic regulation, to better understand the mechanisms underlying these prolonged effects and their implications for long-term growth and metabolic efficiency. Controlled investigations across multiple HS scenarios, particularly in bovine models, are necessary to delineate the precise effects on skeletal muscle physiology and identify potential intervention strategies.

Conclusion

Prenatal heat exposure during late gestation was associated with persistent molecular and cellular differences in skeletal muscle of dairy heifers. Although IUHS calves were lighter at birth, ST muscle mass relative to body weight was maintained through the postweaning period. Across postnatal development, IUHS heifers exhibited altered temporal regulation of stress- and metabolism-related markers, including HSP70 and ATF4, as well as differences in the developmental trajectory of MYH2 expression without consistent treatment differences at all time points. In addition, IUHS heifers displayed greater $PAX7^{+}$ satellite-cell abundance and differences in muscle fiber-type composition at d 63. Collectively, these findings indicate that late-gestation prenatal heat exposure modifies postnatal regulation of skeletal muscle gene, protein expression, and muscle cellular characteristics. However, because mitochondrial function, stress responsiveness, and muscle metabolic capacity were not directly assessed, the functional consequences of these molecular alterations remain to be determined. Further studies integrating longitudinal sampling and functional measurements are required to define how prenatal heat exposure influences skeletal muscle physiology and growth performance later in life.

Conflict of Interest

The authors declare that they have no known competing financial interests or personal relationships that could have appeared to influence the work reported in this paper.

Acknowledgments

Funding for this study was provided by the Hatch project of Michigan State University (Project number MICL027320), awarded to J. Kim, and the US Department of Agriculture National Institute of Food and Agriculture's Agriculture and Food Research Initiative Foundational Program Award 2019-67015-29445 awarded to J. Laporta. We would like to thank Dr. G. E. Dahl and Dr. T. Scheffler (University of Florida), along with the graduate students, for their assistance with euthanasia procedures and sample collection.

Author Contribution

Donghun Kang: data curation, formal analysis, methodology, visualization, and writing—original draft; Erika Eckhardt: investigation, writing—original draft review, and writing—review and editing; Jimena Laporta: conceptualization, supervision, project administration, funding acquisition, and writing—review and editing; Jongkyoo Kim: conceptualization, funding acquisition, project administration, supervision, visualization, and writing—original draft, writing—review and editing; and Sena Field: experimentation—sample collection, processing, and investigation.

Literature Cited

Abu Shelbayeh, O., T. Arroum, S. Morris, and K. B. Busch. 2023. PGC-1α is a master regulator of mitochondrial lifecycle and ROS stress response. Antioxidants. 12:1075. https://doi.org/10.3390/antiox12051075

Ahmed, B. M. S., U. Younas, T. O. Asar, A. P. A. Monteiro, M. J. Hayen, S. Tao, and G. E. Dahl. 2021. Maternal heat stress reduces body and organ growth in calves: Relationship to immune status. JDS communications. 2:295–299.

Barone, R., F. Macaluso, C. Sangiorgi, C. Campanella, A. Marino Gammazza, V. Moresi, D. Coletti, E. Conway de Macario, A. J. L. Macario, F. Cappello, S. Adamo, F. Farina, G. Zummo, and V. Di Felice. 2016. Skeletal muscle heat shock protein 60 increases after endurance training and induces *peroxisome proliferator-activated receptor gamma coactivator 1 α1* expression. Sci. Rep. 6:19781. https://doi.org/10.1038/srep19781

Boddicker, R. L., J. T. Seibert, J. S. Johnson, S. C. Pearce, J. T. Selsby, N. K. Gabler, M. C. Lucy, T. J. Safranski, R. P. Rhoads, L. H. Baumgard, and Jason W. Ross. 2014. Gestational heat stress alters postnatal offspring body composition indices and metabolic parameters in pigs. PLoS One. 9: e110859. https://doi.org/10.1371/journal.pone.0110859

Bosma, M., L. M. Sparks, G. J. Hooiveld, J. A. Jorgensen, S. M. Houten, P. Schrauwen, S. Kersten, and M. K. C. Hesselink. 2013. Overexpression of PLIN5 in skeletal muscle promotes oxidative gene expression and intramyocellular lipid content without compromising insulin sensitivity. Biochim. Biophys. Acta. 1831:844–852. https://doi.org/10.1016/j.bbalip.2013.01.007

Brito, L. F., A. P. Schinckel, and H. R. de Oliveira. 2025. Genomics and phenomics: who will be the dairy cows of the future? JDS Communications. 6:S23–S30. https://doi.org/10.3168/jdsc.2025-0872

Cartwright, S. L., J. Schmied, N. Karrow, and B. A. Mallard. 2023. Impact of heat stress on dairy cattle and selection strategies for thermotolerance: a review. Front. Vet. Sci. 10:1198697. https://doi.org/10.3389/fvets.2023.1198697

Dado-Senn, B., S. L. Field, B. D. Davidson, L. T. Casarotto, M. G. Marrero, V. Ouellet, F. Cunha, M. A. Sacher, C. L. Rice, F. P. Maunsell, G. E. Dahl, and J. Laporta. 2021. Late-gestation *in utero* heat stress limits dairy heifer early-life growth and organ development. Front. Anim. Sci. 2:750390. https://doi.org/10.3389/fanim.2021.750390

Dado-Senn, B. M., S. L. Field, B. D. Davidson, G. E. Dahl, and J. Laporta. 2022. In utero hyperthermia in late gestation derails dairy calf early-life mammary development. J. Anim. Sci. 100:skac186. https://doi.org/10.1093/jas/skac186

Das, R., L. Salio, N. Verma, P. Bharti, J. Saikia, Imtiwati, and R. Kumar. 2016. Impact of heat stress on health and performance of dairy animals: a review. Veterinary World. 12:260–268. https://doi.org/10.14202/vetworld.2016.260-268

Fennel, Z. J., J. B. Ducharme, Q. N. Berkemeier, J. W. Specht, Z. J. McKenna, S. E. Simpson, R. C. Nava, K. A. Escobar, P. S. Hafen, M. R. Deyhle, F. T. Amorim, and C. M. Mermier. 2023. Effect of heat stress on heat shock protein expression and hypertrophy-related signaling in the skeletal muscle of trained individuals. Am. J. Physiol. Regul. Integr. Comp. Physiol. 325:R735–R749. https://doi.org/10.1152/ajpregu.00031.2023

Frier, B. C., and M. Locke. 2007. Heat stress inhibits skeletal muscle hypertrophy. Cell Stress Chaperones. 12:132–141. https://doi.org/10.1379/csc-233r.1

Ganesan, S., C. M. Summers, S. C. Pearce, N. K. Gabler, R. J. Valentine, L. H. Baumgard, R. P. Rhoads, and J. T. Selsby. 2017. Short-term heat stress causes altered intracellular signaling in oxidative skeletal muscle. J. Anim. Sci. 95:2438–2451. https://doi.org/10.2527/jas.2016.1233

Gao, C.-q., Y.-l. Zhao, H.-c. Li, W.-g. Sui, H.-c. Yan, and X.-q. Wang. 2015. Heat stress inhibits proliferation, promotes growth, and induces apoptosis in cultured Lantang swine skeletal muscle satellite cells. J. Zhejiang Univ.-Sci. B. 16:549–559. https://doi.org/10.1631/jzus.B1400339

Guan, B., Y. Liu, B. Xie, S. Zhao, A. Yalikun, W. Chen, M. Zhou, Q. Gu, and D. Yan. 2024. Mitochondrial genome transfer drives metabolic reprogramming in adjacent colonic epithelial cells promoting TGFβ1-mediated tumor progression. Nat. Commun. 15:3653. https://doi.org/10.1038/s41467-024-48100-y

Hafen, P. S., C. N. Preece, J. R. Sorensen, C. R. Hancock, and R. D. Hyldahl. 2018. Repeated exposure to heat stress induces mitochondrial adaptation in human skeletal muscle. J. Appl. Physiol. 125:1447–1455. https://doi.org/10.1152/japplphysiol.00383.2018

Halevy, O., A. Krispin, Y. Leshem, J. P. McMurtry, and S. Yahav. 2001. Early-age heat exposure affects skeletal muscle satellite cell proliferation and differentiation in chicks. Am. J. Physiol. Regul. Integr. Comp. Physiol. 281:R302–R309. https://doi.org/10.1152/ajpregu.2001.281.1.R302

Hernández-Hernández, J. M., E. G. García-González, C. E. Brun, and M. A. Rudnicki. 2017. The myogenic regulatory factors, determinants of muscle development, cell identity and regeneration. Semin. Cell Dev. Biol. 72:10–18. https://doi.org/10.1016/j.semcdb.2017.11.010

Jäger, S., C. Handschin, J. St-Pierre, and B. M. Spiegelman. 2007. AMP-activated protein kinase (AMPK) action in skeletal muscle via direct phosphorylation of PGC-1α. Proc. Natl. Acad. Sci. U.S.A. 104:12017–12022. https://doi.org/10.1073/pnas.0705070104

Johnson, J. S., K. R. Stewart, T. J. Safranski, J. W. Ross, and L. H. Baumgard. 2020. *In utero* heat stress alters postnatal phenotypes in swine. Theriogenology. 154:110–119. https://doi.org/10.1016/j.theriogenology.2020.05.013

Kang, C., and L. L. Ji. 2012. Role of PGC-1α signaling in skeletal muscle health and disease. Ann. N. Y. Acad. Sci. 1271:110–117. https://doi.org/10.1111/j.1749-6632.2012.06738.x

Keerthiga, R., D.-S. Pei, and A. Fu. 2021. Mitochondrial dysfunction, UPR^{mt} signaling, and targeted therapy in metastasis tumor. Cell Biosci. 11:186. https://doi.org/10.1186/s13578-021-00696-0

Kim, J., K. B. Wellmann, Z. K. Smith, and B. J. Johnson. 2018. All-trans retinoic acid increases the expression of oxidative myosin heavy chain through the PPARδ pathway in bovine muscle cells derived from satellite cells. J. Anim. Sci. 96:2763–2776. https://doi.org/10.1093/jas/sky155

Kim, W. S., J. R. Daddam, B. H. Keng, J. Kim, and J. Kim. 2023. Heat shock protein 27 regulates myogenic and self-renewal potential of bovine satellite cells under heat stress. J. Anim. Sci. 101:skad303. https://doi.org/10.1093/jas/skad303

Kim, W. S., and J. Kim. 2023. Exploring the impact of temporal heat stress on skeletal muscle hypertrophy in bovine myocytes. J. Therm. Biol. 117:103684. https://doi.org/10.1016/j.jtherbio.2023.103684

Knutti, D., and A. Kralli. 2001. PGC-1, a versatile coactivator. Trends Endocrinol. Metab. 12:360–365. https://doi.org/10.1016/s1043-2760(01)00457-x

Kuo, T., C. A. Harris, and J.-C. Wang. 2013. Metabolic functions of glucocorticoid receptor in skeletal muscle. Mol. Cell. Endocrinol. 380:79–88. https://doi.org/10.1016/j.mce.2013.03.003

Laporta, J., and M. C. Guenther. 2025. Making future udders: Mammary development and perinatal programming of dairy cattle. JDS communications. 6:S42–S46. https://doi.org/10.3168/jdsc.2025-0828

Li, B., J. Shin, and K. Lee. 2009. Interferon-stimulated gene ISG12b1 inhibits adipogenic differentiation and mitochondrial biogenesis in 3T3-L1 cells. Endocrinology. 150:1217–1224. https://doi.org/10.1210/en.2008-0727

Lucy, M. C., and T. J. Safranski. 2017. Heat stress in pregnant sows: thermal responses and subsequent performance of sows and their offspring. Mol. Reprod. Dev. 84:946–956. https://doi.org/10.1002/mrd.22844

Ma, B., X. He, Z. Lu, L. Zhang, J. Li, Y. Jiang, G. Zhou, and F. Gao. 2018. Chronic heat stress affects muscle hypertrophy, muscle protein synthesis and uptake of amino acid in broilers via insulin like growth factor-mammalian target of rapamycin signal pathway. Poult. Sci. 97:4150–4158. https://doi.org/10.3382/ps/pey291

Marino Gammazza, A., F. Macaluso, V. Di Felice, F. Cappello, and R. Barone. 2018. Hsp60 in skeletal muscle fiber biogenesis and homeostasis: from physical exercise to skeletal muscle pathology. Cells. 7:224. https://doi.org/10.3390/cells7120224

Monteiro, A. P. A., S. Tao, I. M. T. Thompson, and G. E. Dahi. 2016. In utero heat stress decreases calf survival and performance through the first lactation. J. Dairy. Sci. 99:8443–8450. https://doi

Montilla, S. I. R., T. P. Johnson, S. C. Pearce, D. Gardan-Salmon, N. K. Gabler, J. W. Ross, R. P. Rhoads, L. H. Baumgard, S. M.

Lonergan, and J. T. Selsby. 2014. Heat stress causes oxidative stress but not inflammatory signaling in porcine skeletal muscle. Temperature. 1:42–50. https://doi.org/10.4161/temp.28844

Moresi, V., G. Garcia-Alvarez, A. Pristerà, E. Rizzuto, M. C. Albertini, M. Rocchi, G. Marazzi, D. Sassoon, S. Adamo, and D. Coletti. 2009. Modulation of caspase activity regulates skeletal muscle regeneration and function in response to vasopressin and tumor necrosis factor. PLoS One. 4:e5570. https://doi.org/10.1371/journal.pone.0005570

Muñoz-Carvajal, F., and M. Sanhueza. 2020. The mitochondrial unfolded protein response: a hinge between healthy and pathological aging. Front. Aging Neurosci. 12:581849. https://doi.org/10.3389/fnagi.2020.581849

Olguín, H. C., and A. Pisconti. 2012. Marking the tempo for myogenesis: Pax7 and the regulation of muscle stem cell fate decisions. J. Cell. Mol. Med. 16:1013–1025. https://doi.org/10.1111/j.1582-4934.2011.01348.x

Pereyra, A. S., C.-T. Lin, D. M. Sanchez, J. Laskin, E. E. Spangenburg, P. D. Neufer, K. Fisher-Wellman, and J. M. Ellis. 2022. Skeletal muscle undergoes fiber type metabolic switch without myosin heavy chain switch in response to defective fatty acid oxidation. Mol. Metab. 59:101456. https://doi.org/10.1016/j.molmet.2022.101456

Pereira, J. M. V., F. C. Ferreira, P. H. V. Carvalho, J. Bittar, N. S. Del-Rio, and M. I. Marcondes. 2024. Association of morbidity, mortality, and average daily gain with transfer of passive immunity in dairy-beef crossbred calves up to 60 days of life. J. Dairy Sci. 107:8223–8233. https://doi.org/10.3168/jds.2023-24557

Piestun, Y., T. Patael, S. Yahav, S. G. Velleman, and O. Halevy. 2017. Early posthatch thermal stress affects breast muscle development and satellite cell growth and characteristics in broilers. Poult. Sci. 96:2877–2888. https://doi.org/10.3382/ps/pex065

Reith, R. R., R. L. Sieck, P. C. Grijalva, R. M. Swanson, A. M. Fuller, D. E. Diaz, T. B. Schmidt, D. T. Yates, and J. L. Petersen. 2022. Transcriptome analyses indicate that heat stress-induced inflammation in white adipose tissue and oxidative stress in skeletal muscle is partially moderated by zilpaterol supplementation in beef cattle. J. Anim. Sci. 100: skac019. https://doi.org/10.1093/jas/skac019

Senf, S. M., T. M. Howard, B. Ahn, L. F. Ferreira, and A. R. Judge. 2013. Loss of the inducible Hsp70 delays the inflammatory response to skeletal muscle injury and severely impairs muscle regeneration. PLoS One. 8:e62687. https://doi.org/10.1371/journal.pone.0062687

Skibiel, A. L., F. Peñagaricano, R. Amorín, B. M. Ahmed, G. E. Dahl, and J. Laporta. 2018. In utero heat stress alters the offspring epigenome. Sci. Rep. 8:14609. https://doi.org/10.1038/s41598-018-32975-1

Smith, Z. K., E. Eckhardt, W. S. Kim, A. C. B. Menezes, W. C. Rusche, and J. Kim. 2023. Temperature fluctuations modulate molecular mechanisms in skeletal muscle and influence growth potential in beef steers. J. Anim. Sci. 101: skad343. https://doi.org/10.1093/jas/skad343

St-Pierre, J., S. Drori, M. Uldry, J. M. Silvaggi, J. Rhee, S. Jäger, C. Handschin, K. Zheng, J. Lin, W. Yang, D. K. Simon, R. Bachoo, and B. R. Spiegelman. 2006. Suppression of reactive oxygen species and neurodegeneration by the PGC-1 transcriptional coactivators. Cell. 127:397–408. https://doi.org/10.1016/j.cell.2006.09.024

Summer, A., I. Lora, P. Formaggioni, and F. Gottardo. 2019. Impact of heat stress on milk and meat production. Anim. Front. 9:39–46. https://doi.org/10.1093/af/vfy026

Thornton, P., G. Nelson, D. Mayberry, and M. Herrero. 2021. Increases in extreme heat stress in domesticated livestock species during the twenty-first century. Global Ghange Biology. 27:5762–5772. https://doi.org/10.1111/gcb.15825

Uehara, K., K. Goto, T. Kobayashi, A. Kojima, T. Akema, T. Sugiura, S. Yamada, Y. Ohira, T. Yoshioka, and H. Aoki. 2004. Heat-stress enhances proliferative potential in rat soleus muscle. The Japanese Journal of Physiology. 54:263–271. https://doi.org/10.2170/jjphysiol.54.263

Xu, J., G. M. Strasburg, K. M. Reed, and S. G. Velleman. 2022. Thermal stress affects proliferation and differentiation of turkey satellite cells through the mTOR/S6K pathway in a growth-dependent manner. PLoS One. 17:e0262576. https://doi.org/10.1371/journal.pone.0262576

Zammit, P. S. 2017. Function of the myogenic regulatory factors Myf5, MyoD, myogenin and MRF4 in skeletal muscle, satellite cells and regenerative myogenesis. Semin. Cell Dev. Biol. 72:19–32. https://doi.org/10.1016/j.semcdb.2017.11.011